

Anomalous losses of deuterium–deuterium fusion products in the Tokamak Fusion Test Reactor*

S. J. Zweben,[†] C. E. Bush,^{a)} C. S. Chang,^{b)} Z. Chang,^{c)} D. S. Darrow, E. D. Fredrickson, H. W. Herrmann, H. E. Mynick, J. Schivell, M. Bell, R. Boivin,^{d)} R. V. Budny, C. Z. Cheng, D. Ernst,^{d)} G. Hammett, L. C. Johnson, D. McCune, M. Murakami,^{a)} D. K. Owens, J. Park, C.-K. Phillips, M. H. Redi, S. Scott, J. D. Strachan, G. Taylor, M. Tuszewski,^{e)} R. B. White, J. R. Wilson, and M. Zarnstorff

Princeton Plasma Physics Laboratory, P.O. Box 451, Princeton, New Jersey 08543

(Received 3 November 1993; accepted 8 December 1993)

In the Tokamak Fusion Test Reactor (TFTR) [*International Conference on Plasma Physics and Controlled Nuclear Fusion Research*, Wurzburg, Paper No. A-2-2 (International Atomic Energy Agency, Vienna, 1993)] there have been at least three types of anomalous loss of alpha-like deuterium–deuterium (D–D) fusion products: (1) a magnetohydrodynamic (MHD)-induced loss of D–D fusion products correlated with Mirnov and fishbone-type oscillations and sawtooth crashes, (2) a slow “delayed” loss of partially thermalized D–D fusion products occurring without large MHD activity, and (3) ion cyclotron resonance heating (ICRH)-induced loss of D–D fusion products ions observed during direct electron heating experiments, and possibly also during ³He minority heating. In this paper each of these will be reviewed, concentrating on those due to MHD activity, which are the largest of these anomalous losses. The experimental results are compared with numerical models of various fusion product transport mechanisms.

I. INTRODUCTION

In this paper we describe recent measurements and modeling of deuterium–deuterium (D–D) fusion product loss in the Tokamak Fusion Test Reactor (TFTR).¹ The D–D fusion products measured here are the 3 MeV proton and the 1 MeV triton, both of which have a gyroradius and collisionality similar to 3.5 MeV alphas from deuterium–tritium (D–T) reactions. The main goal of these studies is to identify the “single-particle” loss mechanisms for D–D fusion products in TFTR in order to help isolate any new “collective” alpha loss mechanisms that might occur during the upcoming D–T run. Another goal is to identify potentially damaging single-particle alpha loss mechanisms in the International Tokamak Experimental Reactor (ITER) or other tokamak reactors, where even a few percent fast alpha loss may cause damage due to localized heating of the first wall or divertor plate.

Three different types of anomalous fusion product loss are described in this paper: namely, loss due to magnetohydrodynamic (MHD) activity, delayed loss, and loss due to ion cyclotron resonance heating (ICRH). These processes are anomalous, in the sense that they are not yet understood quantitatively, and so are not yet included in calculations of alpha loss in future D–T reactors. The emphasis here will be on the largest of these losses, namely that due to conventional MHD activity. Note that previous measurements and modeling of D–D fusion product loss in

TFTR have identified both the “classical” first-orbit loss² and the stochastic toroidal field (TF) ripple-induced loss,^{3,4} which form an experimental baseline from which these anomalous loss processes can be evaluated.

The measurements described below were all made during the 1992 TFTR D–D run using the Lost Alpha diagnostic (Sec. II), which will also be used to measure alpha loss during the deuterium–tritium (D–T) run. The theory and modeling come from several sources, including guiding center Monte Carlo codes and simplified analytical modeling. Although some of these results have already been summarized at a recent conference,⁵ in this paper there is more detailed data on MHD-induced loss during $\frac{3}{2}$ -type and fishbone-type modes, improved modeling of $\frac{3}{2}$ -type MHD-induced loss, and the first discussion of classical pitch angle scattering as a possible cause of the delayed loss.

II. THE LOST ALPHA DIAGNOSTIC

The “Lost Alpha” diagnostic on TFTR was designed to measure alpha loss in D–T plasmas, but can also measure loss of D–D fusion products, which is ≈ 100 times smaller. Since 1990 there have been four detectors installed in a poloidal array at angles of 90°, 60°, 45°, and 20° below the outer midplane. The first three of these are fixed in position with their apertures 1 cm radially outside the radius of the poloidal ring limiters (which have a minor radius of 0.99 m from their center at a major radius of $R=2.61$ m, but which are displaced ≥ 2 m toroidally from these detectors). The 20° or “midplane” detector is mounted on a probe shaft that is radially movable to well inside the limiter radius.

Each of these detectors has a pair of apertures designed to disperse ions according to their gyroradius (energy) in

*Paper 515, Bull. Am. Phys. Soc. 38, 1985 (1993).

[†]Invited speaker.

^{a)}Oak Ridge National Laboratory, Oak Ridge, Tennessee 08543.

^{b)}New York University, New York City, New York 10012.

^{c)}University of Wisconsin, Madison, Wisconsin 53706.

^{d)}Massachusetts Institute of Technology, Cambridge, Massachusetts 02139.

^{e)}Los Alamos National Laboratory, Los Alamos, New Mexico 87545.

one direction and their pitch angle (magnetic moment) in the other direction. After passing through the apertures, the fast ions strike a thin layer of inorganic crystal phosphor, which was a 18 μm layer of P31 (ZnS[Cu]) for the experiments of the 1992 run. The resulting scintillation light image is focused onto a coherent quartz fiber optic bundle and carried to detectors in a shielded area. For D–D plasmas these scintillators are primarily sensitive to 3 MeV protons ($\approx 60\%$ of the light output), and 1 MeV tritons ($\approx 40\%$ of the light output), whereas the 0.8 MeV ^3He fusion product is filtered out by a 3 μm aluminum foil that covers the inner aperture.^{2,6} Since the protons and tritons have exactly the same gyroradius at birth, for most of the discussion below they are lumped together as “D–D fusion products” (even though they do have somewhat different collisionality).

The visible light images from these scintillators are monitored by an intensified video camera in parallel with a set of photomultiplier (PM) tubes. The camera is used for recording the 2-D images of the scintillators for analyzing the pitch angle versus gyroradius distribution, typically at 16 or 33 frames/s. For the 1992 run, the total light output from each detector was also sent to individual PM tubes in order to examine the time dependence with a time response of $\approx 20 \mu\text{s}$. This is similar to the $1/e$ decay time of the light from the P31 scintillators used in 1992.⁷

Energy resolution is limited in these detectors, since it is set by the geometrical resolution of the aperture pair (as in an unfocused magnetic spectrometer), and not by the detector itself (as in a silicon detector pulse height analysis system). Furthermore, only the ion gyroradius distribution can be determined and not the ion species, which has caused some ambiguity in ICRH minority heating experiments with multiple fast ion species. The measured gyroradius distribution is fit by model curves generated by a detector simulation code, which can determine relative changes in the ion energy of about ± 1 MeV for 3 MeV protons. This is good enough to distinguish the delayed loss at about half the birth energy, but not good enough to determine its detailed energy spectrum.

The absolute calibration of these detectors has been uncertain by about a factor of 2 or 3,⁶ which is not very good compared to the uncertainty of about $\pm 10\%$ – 20% of global neutron source measurements. This is due to a combination of several factors, including uncertainties in the light output per MeV ion, in the angular distribution of this light output, and in the optical throughput of the of the lenses and fiber bundles. The scintillator calibration work using the Los Alamos Van de Graaff⁷ is presently being extended to provide a more accurate absolute calibration.

III. EXPERIMENTAL RESULTS ON MHD-INDUCED LOSS

The first evidence of MHD-induced loss of D–D fusion products in TFTR came shortly after the array of 2-D imaging scintillator detectors was installed, when increases in the fusion product loss by a factor of ≈ 3 were seen in the 90° detector at times of large MHD activity.⁸ This

increased loss fluctuated in time with the frequency of the MHD activity in the range ≈ 2 Hz (nearly locked modes) to ≈ 5 kHz (Mirnov oscillations in rotating plasmas).

Every TFTR run since then has had many discharges with very similar symptoms of MHD-induced loss, particularly at high neutral beam injection (NBI) power and at high current ($I > 1.4$ MA). The results for discharges in the current range $I = 1.6$ – 2.0 MA can be summarized as follows:^{5,9} (a) the D–D fusion product loss in the 90° detector (normalized by the instantaneous neutron rate) can increase during strong MHD activity by up to a factor of ≈ 3 – 5 above the MHD-quiescent level; (b) these increased loss rates seem to persist as long as the MHD activity lasts, which is often longer than the 3 MeV proton slowing-down time of ≈ 0.2 s; (c) this extra loss due to MHD activity can increase the total loss up to the level of first-orbit loss at $I = 0.8$ MA, i.e., up to an estimated level of $\approx 20\%$ – 30% globally; (d) the MHD-induced loss is often observed to be strongly modulated with the MHD up to a frequency of ≈ 5 kHz, with instantaneous peak loss rates up to about ten times the “baseline” level without MHD; and (e) qualitatively similar MHD-induced loss has been seen in all four detectors for all plasma major radii in the normal range of TFTR plasmas $I = 1$ – 2 MA and $R = 2.45$ – 2.62 m.

Two examples of MHD-induced D–D fusion product loss as measured during the 1992 run are shown in Fig. 1, taken from an experiment designed to examine the effect of the plasma current profile on MHD activity and fusion reactivity in supershots. For all discharges in this experiment the plasma current was $I \approx 1.6$ – 1.65 MA, the toroidal field on axis was $B_T = 4.8$ T, $q(0) \approx 0.8 \pm 0.2$, $q(a) \approx 5$ (Shafranov), the plasma major radius was $R = 2.45$ m, and the NBI power was 24 MW from 3–4 s. The fusion product loss signals shown in Fig. 1 were taken from the PM tubes monitoring the total scintillator light from each detector (the neutron/gamma backgrounds were negligible in these cases). The 20° detector escaping alpha was inserted with its aperture 3.5 cm inside the limiter radius (but still well outside the plasma edge) for both these shots.

One of the discharges in Fig. 1 had relatively large and gradually increasing $m = 3$, $n = 2$ mode activity from about ≈ 3.25 to 4.0 s (#66869), which correlated with a degradation in plasma confinement and neutron rate from ≈ 3.5 – 4.0 s. The other discharge was relatively MHD quiescent, but did have “fishbone-type” $m = 1$, $n = 1$ MHD activity from ≈ 3.45 – 4.0 s (#66896), which apparently did not affect the global plasma confinement or neutron rate. Under these plasma conditions there was a consistent correlation between the high $\frac{3}{2}$ mode activity and anomalously high fusion product loss, with lower fusion product loss consistently observed during $\frac{4}{3}$ -mode activity, and the lowest loss (for these 24 MW shots) during discharges with 1/1-mode fishbone activity.¹⁰ This type of MHD-induced loss is quite reproducible and persistent in high-powered supershots with $R = 2.45$ m and $I = 1.4$ – 1.8 MA.

For the typical cases shown in Fig. 1, the $\frac{3}{2}$ -type discharge at ≈ 3.8 s showed a fusion product loss rate (per neutron) in the 90° detector which was ≈ 2.5 times higher

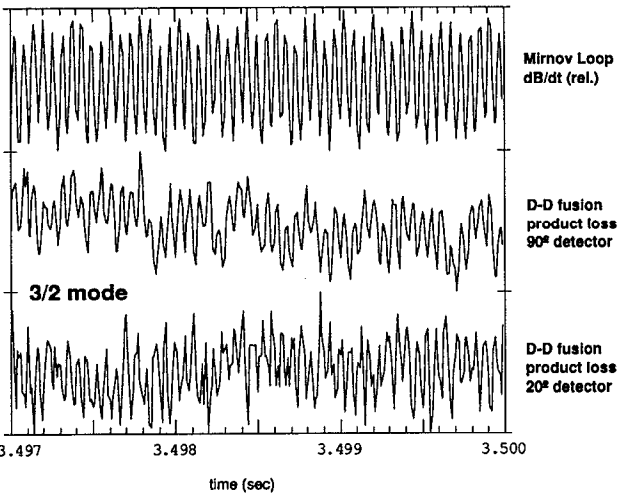
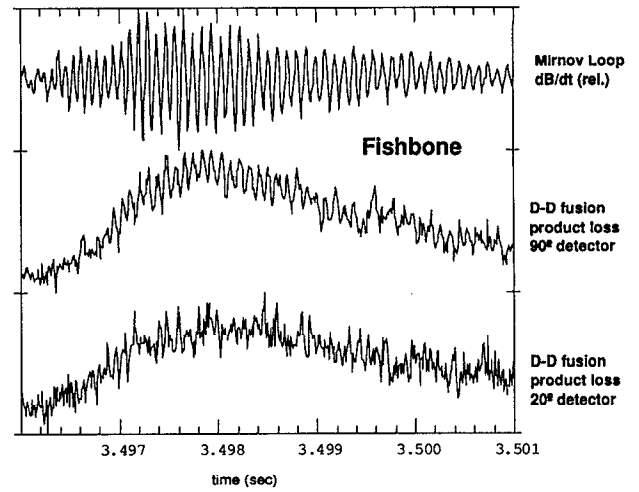
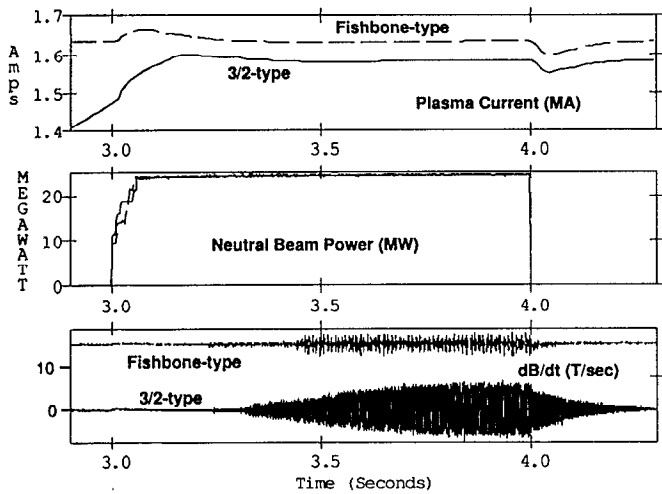


FIG. 1. MHD-induced loss of D-D fusion products during NBI for $R=2.45$ m, $I=1.6$ MA, 24 MW NBI discharges in TFTR. These shots differ in their type of MHD activity, most likely due to the different plasma current evolution before NBI (and not the slightly different final current). The MHD-induced loss in the fishbone-type shot (#66896) starts at about 3.45 s, while the MHD-induced loss in the $\frac{3}{2}$ -type shot (#66869) appears to start at ≈ 3.25 s. The D-D fusion product loss at both the 90° and 20° (midplane) detectors increases by $\approx 20\%$ at each fishbone, and by $\approx 2-3$ above the MHD-quiescent level during $\frac{3}{2}$ -type MHD. Without the MHD activity, the escaping fusion product signals at 90° follows the time dependence of the first-orbit loss early in time (< 0.2 s), with delayed loss dominating the signals later. The Mirnov signals are taken from a coil at the vessel wall near the outer midplane.

than for the fishbone-type discharge. The corresponding ratio in the 20° detector was ≈ 3.6 at the same time, while for the 60° and 45° detectors the ratio of the loss between $\frac{3}{2}$ -type and fishbone-type discharges was a factor of ≈ 1.5 and ≈ 1.3 , respectively. Thus the poloidally averaged fusion product loss over the range 20°–90° below the outer midplane was increased by ≈ 2 during $\frac{3}{2}$ -type MHD activity, when compared to the relatively MHD-quiescent fishbone-type discharge. There was also a slight ($\approx 20\%$) increase in the fusion product loss at each fishbone, starting from the first one at ≈ 3.45 s and continuing simultaneously in both the 90° and 20° detectors, as long as the fishbone-type MHD lasts (> 0.5 s).

These same signals are shown on an ≈ 5 ms time scale

FIG. 2. Comparison over a time scale of $\approx 3-5$ ms of the MHD activity and fusion product loss for the same two shots shown in Fig. 1. The escaping D-D fusion product signals are only weakly modulated at the fishbone frequency of ≈ 10 kHz, or the $\frac{3}{2}$ mode frequency of ≈ 20 kHz. The inferred amplitude of the magnetic perturbation near the $q=1$ surface during the fishbone is roughly $B_r/B_T \approx 10^{-3}$, and the amplitude of the $\frac{3}{2}$ mode is roughly $B_r/B_T \approx 10^{-4}$ near the $q=\frac{3}{2}$ surface.

in Fig. 2 (at ≈ 3.5 s). For the fishbone-type discharge there is a small but consistent increase in the D-D fusion product loss at each fishbone burst, with a perceptible modulation in the 90° detector at the fishbone frequency of ≈ 10 kHz (less clear in the 20° detector). The fishbone-induced fusion product loss follows closely in time the envelope of the Mirnov signal at both the 90° and 45° detectors, with the peak loss coinciding with the peak fluctuation level to within < 1 ms (even at the first fishbone), suggesting that this loss process is very rapid compared to the thermal energy confinement time of ≈ 150 ms. For the $\frac{3}{2}$ -type discharge there is a few percent (RMS) modulation of the loss at both detectors at the $\frac{3}{2}$ mode frequency of ≈ 20 kHz. The amplitude of these modulations approximately follows the amplitude of the Mirnov signal over the time scale of the NBI. Note that the $1/e$ decay time of the P31 scintillator is ≈ 20 μ s,⁷ which tends to reduce the fluctuation level somewhat at frequencies ≥ 20 kHz.

The pitch angle and gyroradius distributions of the loss

for these same discharges have been analyzed for the 90° detector.⁹ During fishbone activity, the additional loss usually appears to be localized at a pitch angle near the passing/trapped boundary, i.e., near the fattest banana orbit. The pitch angle distribution of the loss during the $\frac{3}{2}$ -type activity is more similar to that observed without MHD activity, with a slight tendency for additional loss toward high pitch angles corresponding to trapped ions fairly far from the passing/trapped boundary. This suggests that the MHD-induced loss to the 90° detector consists of both passing ions (lost across the passing/trapped boundary), and also trapped ions (though not necessarily at exactly the same time). The gyroradius distribution of the loss during fishbone activity is nearly the same as the loss before or between fishbones (i.e., including both first-orbit and a delayed loss component), while for the $\frac{3}{2}$ -type discharge the additional loss is usually weighted toward lower gyroradii, corresponding to a lowering of the average loss energy by $\approx 20\%$. The broad instrumental response of this detector makes it difficult to unfold the escaping ion energy distribution more precisely.

The magnitude of the $\frac{3}{2}$ -type anomalous fusion product loss normalized by the instantaneous neutron source rate increases approximately linearly with the magnitude of the magnetic fluctuation amplitude up to ≈ 0.05 G (as measured at the edge), but increases only very slowly between ≈ 0.1 – 0.25 G.¹⁰ For example, in the $\frac{3}{2}$ -type discharge in Fig. 1 the measured edge fluctuation increased from $\tilde{B}_{\text{pol}} \approx 0.05$ G at 3.4 s to $\tilde{B}_{\text{pol}} \approx 0.15$ G at ≈ 3.7 – 4.0 s, whereas the total loss (per neutron) was remained approximately constant over this time. The magnitude of the fishbone-type anomalous fusion product loss increases approximately linearly with the magnitude of the edge magnetic fluctuations during each fishbone, as shown in Fig. 2.

The magnitude of the maximum internal magnetic perturbations near the rational surfaces for these two cases have been estimated from cylindrical linear delta-prime code, which uses the magnetic fluctuations measured just inside the vacuum vessel to determine the theoretical radial eigenmode inside the plasma.¹¹ For these two cases the magnetic analyses were dominated by modes of a single helicity, with a peak fluctuation level of $\tilde{B}_r/B_T \approx 1 \times 10^{-4}$ for the $\frac{3}{2}$ type and $\tilde{B}_r/B_T \approx 1 \times 10^{-3}$ for the (1,1) fishbone-type perturbations, with an estimated uncertainty of about a factor of 2.

The time dependence of the neutron-normalized fusion product loss at 90° for a few other MHD active discharges is shown in Fig. 3. For each of these cases the plasma current, major radius, and NBI power were nearly the same as for Fig. 1 (i.e., $I = 1.65$ MA, $R = 2.45$ m, $P = 18$ MW); however, the details of the time dependence of the $\frac{3}{2}$ -mode levels and resulting MHD-induced fusion product loss vary considerably, as is usually the case in high-powered TFTR discharges. In particular, one of these discharges has a “minor disruption” after just 3.5 s, which increased the fusion product loss level by a factor of 5 within ≈ 10 ms.

MHD-induced loss was also observed during the 1992 TFTR run during sawtooth crashes and just before major

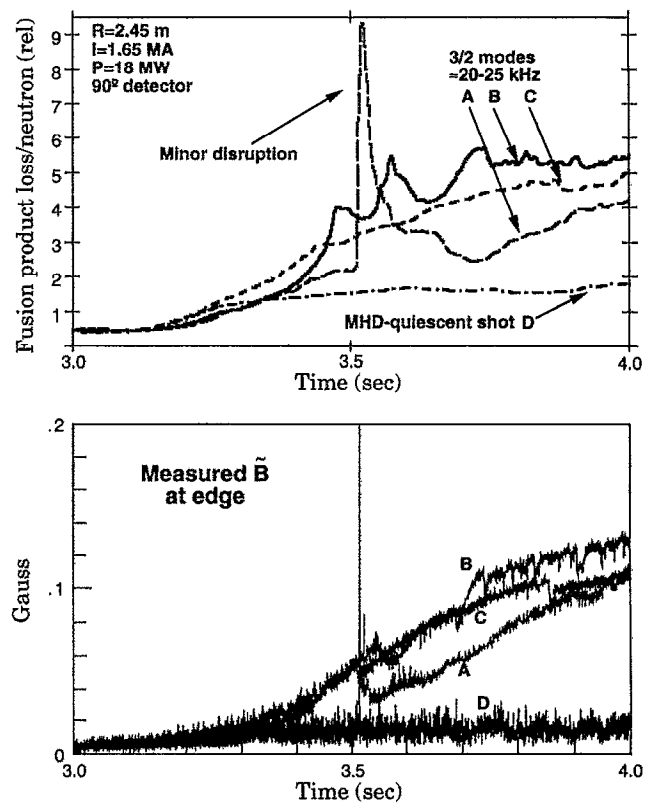


FIG. 3. Other examples of MHD-induced loss at 90° during $\frac{3}{2}$ mode activity, showing the variability of the MHD level and the fusion product loss over time during a shot and from shot-to-shot. One of these discharges had a minor disruption at ≈ 3.5 s, which increased the fusion product loss dramatically.

disruptions.⁵ The loss at sawtooth crashes is usually a fast spike (≈ 10 – 100 μ s wide) localized in pitch angle near the passing/trapped boundary, which can occur at every sawtooth crash during NBI (usually there is no more than one sawtooth crash during NBI in supershots, but several during NBI in L-mode plasmas). A systematic study of these spikes has not yet been made, but they seem to cause a negligible total loss (although they might well redistribute charged fusion products within the plasma). The pre-disruptive MHD-induced loss, which can occur as much as ≈ 50 ms before the plasma current quench, can be up to ≈ 50 times the level of the MHD-quiescent loss rate. This process has been seen to expel up to an estimated $\approx 10\%$ of the existing D–D fusion products over the ≈ 10 ms preceding a current quench; thus this phenomenon could potentially cause a unique wall-loading problem for alpha-heated reactors.

Measurements and modeling of the loss of NBI ions and ICRH tail ions due to collective fast ion MHD instabilities in TFTR D–D are described elsewhere.^{12,13} These collective effects have not yet been studied using actual fusion products in TFTR, but will be a major focus of alpha particle studies during a TFTR run.¹⁴

IV. MODELING OF MHD-INDUCED LOSS

There are several possible mechanisms that could increase the D–D fusion product loss during MHD activity:

(1) modification of the “classical” first-orbit or TF ripple loss due to MHD-induced changes in the fusion product source profile or plasma current profile, (2) magnetic fluctuation-induced radial transport and loss of previously confined fusion products, or (3) indirect MHD-induced effects on some other mechanism of fusion product loss. Note that we are assuming here that the D–D fusion product density and beta are too low to excite collective instabilities, which may not be true for the ≈ 100 times larger population of D–T alphas.

Increased fusion product loss of the first type (1) could, in principle, be due to an MHD-induced increase in the local D–D fusion reaction rate at radii where fusion products are lost through these effects. For example, a $\approx 20\%$ increase in the local source rate at $r/a \approx 0.3$ in $I = 1.6$ MA discharges would cause a $\approx 20\%$ increase in the loss near the fattest banana loss orbits (which can originate from this radius). This could potentially explain the characteristics of the fishbone-induced fusion product loss shown in Figs. 1 and 2. However, to explain the increases seen during $\frac{3}{2}$ -type activity, the local source near $r/a \approx 0.3 \pm 0.1$ would have to increase by $\times 2$ – 3 times above that during the fishbone-type discharge, which is highly unlikely given the global decrease in the global neutron rate. Analysis of the neutron emission profiles for these discharges so far indicates that during MHD activity the source rate generally decreases inside $r/a \approx 0.5$ (but might increase for $r/a > 0.5$).¹⁵

Another “classical” MHD-induced effect could come through any modification of the plasma current profile by the MHD activity, since the current profile affects both the first-orbit and TF ripple losses. However, the calculated effect is small compared to the observed MHD-induced changes (a $\approx 25\%$ decrease is expected between 1.4 and 1.6 MA discharges), and also cannot explain the very rapid increases in fusion product loss correlated with MHD observed in many cases, such as the minor disruption shown in Fig. 3. The classical Stochastic TF ripple loss could also be modified by either source profile or current profile changes, but this should affect mainly the loss to the outer midplane and not to the 90° detector, in contrast to the results of Fig. 1, which show a qualitatively similar MHD-induced loss at both detectors.

The second possible mechanism for MHD-induced loss is the one that we believe to be dominant in these experiments: namely, the magnetic fluctuation-induced radial transport of previously confined fusion products. Recent modeling has aimed to understand the interactions between charged fusion products and helical magnetic islands, which are thought to be a basic component of what we normally call “MHD activity” in tokamaks, and to apply these models to explain the TFTR fusion product loss data, such as described above.

The mechanism of this interaction occurs through perturbed ion drifts across the toroidal field due to the “magnetic flutter” effect (proportional to the local \tilde{B}_r/B_T), and also to grad- B drifts in the perturbed fields (proportional to $\sqrt{(\tilde{B}_r/B_T)}$). There is a threshold level of the perturbed magnetic field above which both passing or

trapped ion orbits can become stochastic.¹⁶ Since this threshold depends on the mixing of the $m=1, n=0$ orbit shift with the m/n structure of the magnetic perturbation, this threshold is generally lower for higher energy ions, which stray farther from the magnetic field lines. Thus fusion product ions are more likely to become stochastic than lower energy neutral beam ions, given the same perturbed magnetic field structure.

This stochastic fast ion motion can cause a very rapid radial transport of fusion products, which could lead to rapid loss if this stochastic particle motion region reaches the wall. However, this MHD-induced stochastic orbit region can also be localized within the plasma where the magnetic perturbation is largest. In contrast, the stochastic TF ripple region¹⁷ generally causes fast ion loss to the wall due to the radially increasing TF ripple strength.

These fast ion orbit perturbations due to assumed helical magnetic perturbations have been incorporated into the guiding center code “GC3,”¹⁶ which has been previously used to model the MHD-induced transport of 3.5 MeV alphas for an $I = 2.0$ MA TFTR test case. An updated version of this same code has been run for a direct comparison with the results of Sec. II, i.e., using 3 MeV protons in TFTR at $I = 1.65$ MA and $R = 2.45$ m for (3,2) modes. The code has been improved by adding the calculated magnetic ripple effect of MHD perturbations on the ∇B drifts, in addition to the magnetic flutter term proportional to \tilde{B}_r/B_T . The modeling of the magnetic field has also been improved to take the $1/R$ into account exactly (previous modeling used a large aspect ratio expansion of B_T , which caused the loss levels to be overestimated). Collisional effects, TF ripple, and the Shafranov shift are still not included.

The radial profiles of the magnetic flutter and ripple terms \tilde{B}_r/B_T and $\delta|B|/B_T$ are compared for the code and the experiment in Figs. 4(a) and 4(b). Evidently the code models the variation of $|B|$ very well (i.e., the MHD-induced ripple term), but it somewhat misses the radial structure of the mode inferred from the MHD instability model. Given these perturbations, the 3 MeV protons were launched with a random pitch angle, poloidal angle, and toroidal angle, with a radial profile proportional to $(1 - [r/a]^2)^8$, which simulates the expected birth distribution of D–D fusion products. The code was run with 500 ions for 5000 transits, which corresponds to ≈ 5 ms of real time (which is still short compared to the proton thermalization time of ≈ 0.2 s).

The results of the code with respect to the global loss of 3 MeV protons are shown in Fig. 5. With both the flutter and ripple terms, the presence of the $\frac{3}{2}$ mode increased the global loss of 3 MeV protons by about a factor of 2 (above the first-orbit loss) at the estimated internal fluctuation level of $\tilde{B}_r/B_T \approx 10^{-4}$ for the $\frac{3}{2}$ mode discharges discussed in Sec. II. This is fairly close to the observed increase of a factor of 3–5 above the first-orbit loss observed in the 90° detector (see Sec. III). Note that the poloidal distribution of the MHD-induced loss cannot be determined by runs with only 500 ions, since only $\approx 2\% \times 500 = 10$ ions are lost; however, special code runs with 2000 ions suggest that

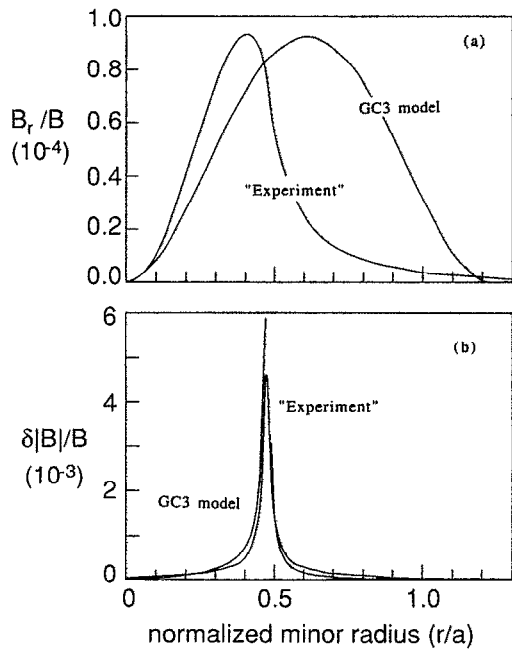


FIG. 4. Comparison of the radial profiles of the magnetic flutter and ripple terms between the experiment and GC3 model for $\frac{3}{2}$ modes in TFTR. The GC3 code accurately models the ripple term (which depends on the magnetic island size), but somewhat misses the radial profile of the radial magnetic perturbation, as estimated for the actual experimental conditions.

the poloidal distribution of the MHD-induced loss is similar to that of the first-orbit loss at the low levels of $\tilde{B}_r/B_T \approx 10^{-4}$ in the experiment.

There are several inadequacies in the present level of comparison between the observed and calculated loss. First, the estimated internal magnetic fluctuation levels are uncertain, since they are derived from extrapolated edge measurements. Second, it is possible that small additional

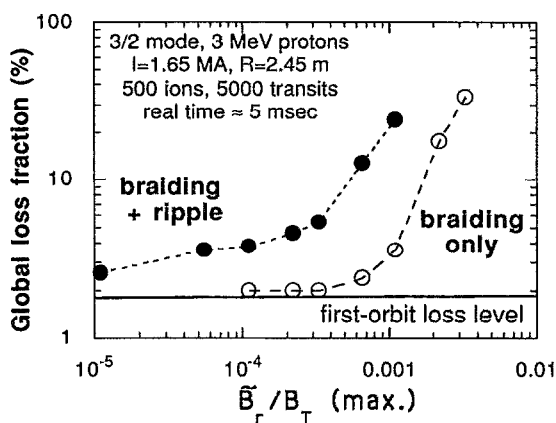


FIG. 5. Results from the GC3 model for the global loss of 3 MeV protons due to a varying $\frac{3}{2}$ mode in TFTR. The estimated level of $\frac{3}{2}$ mode activity in the experimental cases of Figs. 1–3 is $B_r/B_T \approx 10^{-4}$, at which point the calculated MHD-induced loss is approximately the same as the calculated first-orbit loss. The experimental results show a larger MHD-induced loss in the 90° detector.

(m,n) components not measured by the magnetic loops could dramatically increase the calculated loss due to a reduction in the stochastic threshold. Third, the available computer speed presently allows runs to be made for only a small fraction of the fusion product slowing-down time, thus underestimating the total loss somewhat. Other complicating factors include the uncertainties in the plasma current profile and the fusion product source profile (including possible fluctuations in the local source rate due to the MHD itself), and the possible “synergistic” effect of TF ripple and MHD, e.g., wherein MHD-induced loss brings ions out to a radius where the TF ripple causes them to be lost.

The third possible cause of MHD-induced loss mentioned above involves the indirect effect of the MHD on some presently unidentified mechanism of fusion product loss. Such a mechanism is not entirely academic, since an anomalous nonfluctuating “delayed loss” component at about half the birth energy has already been identified in $I=1.6$ MA, $R=2.45$ m discharges (such as those described above), both with or without MHD activity, as described in the next section.

V. EXPERIMENTAL RESULTS ON DELAYED LOSS

The basic experimental results on the “delayed” loss of D–D fusion products were described recently,¹⁸ so here only a summary and a few additional details will be presented. Most of the recent progress in this area has been in the modeling of collisional loss, as discussed in Sec. VI.

The main characteristics of this loss are¹⁸ (1) its appearance is delayed by $\approx 0.2 \pm 0.1$ s with respect to the usual prompt first-orbit loss, as can be seen most clearly at the beginning and end of the NBI; (2) the energy of this loss feature is about half that of the prompt first-orbit loss, as inferred from the gyroradius of its scintillator impact; (3) the strength of this loss feature increased with respect to the first-orbit loss with increased plasma current, and increased with NBI power at a fixed current; (4) the delayed loss at 90° has a strong dependence on the plasma major radius, disappearing at $R > 2.55$ m; and (5) the characteristics of this loss process were very reproducible, occurring on every discharge of this type, except for those with strong MHD activity, when the delayed loss feature in the 90° detector could either increase or decrease with respect to its MHD-quietest level.

An example of delayed loss versus time is shown in Fig. 6 for a typical discharge at $I=1.8$ MA, $R=2.45$ m, and $P=12.4$ MW NBI power. The measured loss normalized to the instantaneous neutron rate increases between ≈ 0.1 and 0.2 s after the start of NBI, and increases still further over 0.2 s just after the NBI ends, showing the delayed nature of the loss. The scintillator light patterns at the bottom of Fig. 6 show how the gyroradius is reduced during the period of delayed loss compared to the pattern at ≈ 0.1 s after NBI (which at 0.1 s is consistent with prompt first-orbit loss). The low energy of the delayed loss is particularly evident just after NBI, when the first-orbit loss level is much reduced.

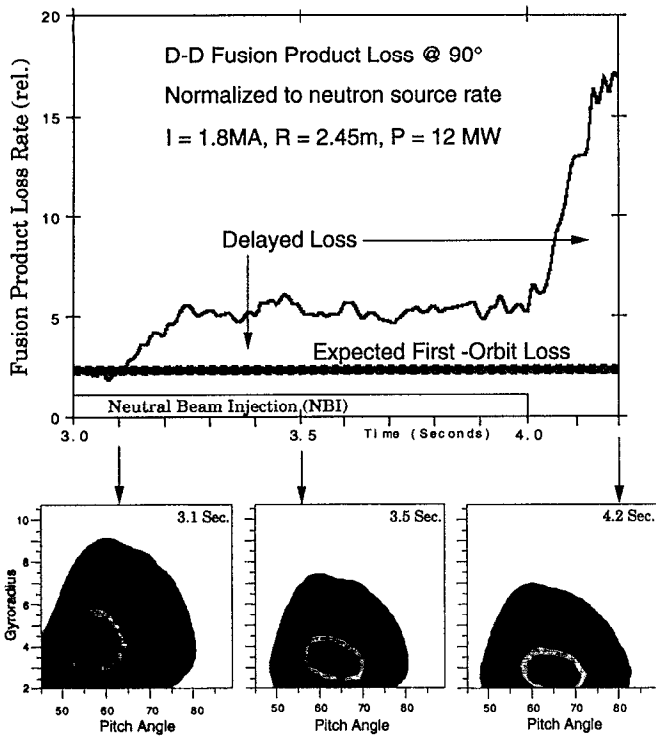


FIG. 6. Delayed loss versus time for a typical $R=2.45$ m TFTR discharge. The observed loss starts to increase above the expected first-orbit level at ≈ 0.1 - 0.2 s, remains ≈ 2 times the expected first-orbit level in this discharge for the whole NBI duration, and increases farther above the first-orbit loss level after NBI ends. The patterns of pitch angle versus gyroradius show that the measured gyroradius is lower during periods of delayed loss than at 0.1 s after the start of NBI, when the gyroradius distribution is consistent with first-orbit loss.

The dependence of the total loss at 90° on NBI power for a set of discharges similar to that of Fig. 6 is shown in Fig. 7. The total loss increases with NBI power mainly due to the delayed loss, while the calculated first-orbit loss stays nearly constant with NBI power (depending mainly

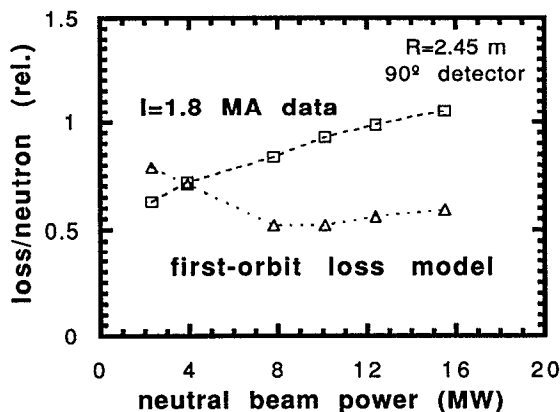


FIG. 7. Variation of the total loss at 90° vs NBI power for discharges similar to that shown in Fig. 6. The total loss increases with NBI due to an increase in the delayed loss, since the calculated first-orbit loss remains constant or falls slightly with NBI due to the variation in the D-D fusion product source profile shape.

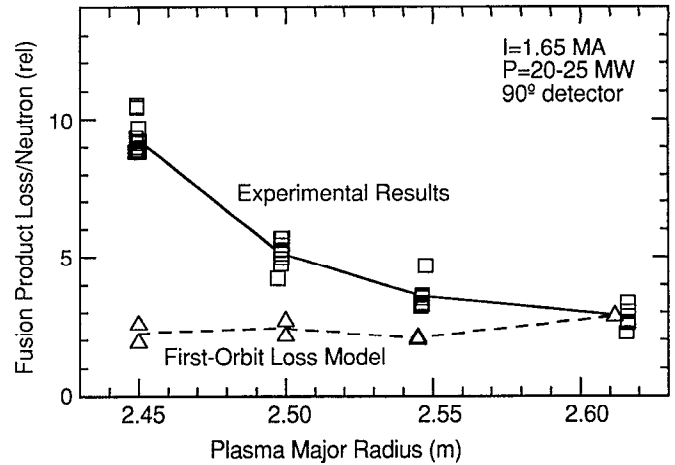


FIG. 8. Variation in the total neutron-normalized loss at 90° versus the major radius of TFTR plasmas with ≈ 20 - 25 MW NBI. The delayed loss increases at this detector for plasmas with smaller major radius. The data is normalized to the first-orbit loss calculations at $R=2.6$ m, where no signs of delayed loss were seen.

on the neutron source profile shape). For this figure the calculated first-orbit loss has been normalized to the measured loss at $I=0.6$ MA where the first-orbit loss is expected to dominate the total loss.²

The major radius dependence of the delayed loss at 90° is shown in Fig. 8 for discharges with $I=1.6 \pm 0.5$ MA and $P \approx 20$ - 25 MW NBI (similar to those of Fig. 1), averaged between ≈ 0.2 - 0.9 s after the start of NBI. The calculated first-orbit loss was normalized to the data at $R=2.6$ m, where no signs of delayed loss were seen.¹⁸ At $R=2.45$ m the delayed loss was nearly four times larger than the calculated first-orbit loss for these high-power discharges.

The very persistent and reproducible nature of this loss suggests that it is not due to conventional MHD activity, which tend to be variable from shot to shot, as shown in Fig. 3. However, the delayed loss can be strongly modulated by such MHD activity, causing it to either increase or decrease.¹⁸

VI. MODELING OF DELAYED LOSS

The very reproducible nature of the delayed loss at 90° suggests that it is caused by some "classical" mechanism, and not to MHD or other variable plasma fluctuations. The observed delay time of ≈ 0.2 s suggests further that this loss might be due to a classical collisional loss mechanism, since this is roughly the time scale for slowing down of fusion products. The axisymmetric collisional losses for fusion products have been thought to be small, since the pitch angle scattering rate is small compared to the slowing down time, and the orbit size is simply reduced by the gradual energy loss without much radial diffusion. However, these calculations have generally been done only in the small banana width limit relevant for high current tokamak reactors.¹⁹

Recently, the expected classical collisional loss for alpha particles in a moderate current axisymmetric tokamak

TABLE I. Fusion product collision rates in TFTR.

	τ_{slow} (velocity e -fold)	τ_{scatt} ($\delta\{v_{\parallel}^2/v^2\}e$ -fold)	$\tau_{\text{slow}}/\tau_{\text{scatt}}$
3 MeV P	≈ 0.4 s	≈ 10 s	≈ 25
1 MeV T	≈ 1.3 s	≈ 3 s	≈ 2
3.5 MeV α	≈ 0.4 s	≈ 6 s	≈ 15

was calculated by the Kiev group,²⁰ based on parameters similar to those of TFTR. They concluded that the presence of a fairly large first-orbit loss cone in plasmas like those of TFTR at $I \approx 1.5$ MA resulted in a surprisingly large amount of loss due to pitch angle scattering of alphas across the passing-trapped loss boundary. This led to an estimated collisional loss of about half the calculated first-orbit loss at 1.5 MA, but this estimate was made for plasma density and temperature profiles much broader than those of TFTR.

The relevant time scales for the slowing down and pitch angle scattering of fusion products in TFTR are shown in Table I, as evaluated at $r/a=0.36$ for a typical $I=1.65$ MA, $R=2.45$ m, $a=0.8$ m, $P=24$ MW plasma, where $n_e \approx 5 \times 10^{13}$ cm⁻³, $T_e \approx 6$ keV, and $Z \approx 3$ (this radius was the midplane crossing radius of the fattest banana orbit for these fusion products). The collisional effects should be largest for the 1 MeV triton, since the ratio of its pitch angle scattering time to slowing down time is ≈ 10 times larger than for 3 MeV protons. The accumulated small-angle scattering over a slowing down time is roughly proportional to the square root of this ratio. Thus, a fairly large fraction of the confined tritons born near the local passing/trapped boundary should be lost due to pitch angle scattering across the passing/trapped boundary (but note that this boundary disappears below about $E/E_0=0.75$ at this radius for these plasmas).

The effects of this type of axisymmetric collisional loss on fusion product confinement in TFTR are routinely evaluated by TRANSP²¹ using its standard Monte Carlo guiding center package. The global loss fraction for 1 MeV tritons due to collisional effects is estimated to be $\approx 0.8\%$ for a standard TFTR supershot at $R=2.45$ m, $I=1.6$ MA, which is $\approx 15\%$ of its calculated first-orbit loss fraction of 5.5% for this shot (#66887). The global loss estimated due to collisions for 3.5 MeV alphas in the same discharge is only $\approx 0.35\%$, which is only $\approx 5\%$ of the calculated first-orbit loss fraction of 7.2% for that shot. The collisional (i.e., delayed) loss in these calculations is located mainly near the passing/trapped boundary in pitch angle, as expected; however, the loss statistics are not good enough for a direct comparison with the measured loss at the 90° detector. The collisional loss of 3.5 MeV alphas has also been calculated recently using an independent guiding center code used for TF ripple loss studies, which predicted an axisymmetric global collisional loss of $\approx 1\%$ in a $R=2.6$ m, $I=1.8$ MA TFTR discharge in which the first-orbit loss was calculated to be $\approx 9\%$.²² Thus, the available Monte Carlo codes predict a relatively small increase in the global alpha particle loss fraction due to collisional effects.

In comparison, the global loss of alphas due to collisionless stochastic TF ripple loss alone is estimated to be $\approx 3\%–8\%$ for $I=1.6–1.8$ MA at $R=2.45–2.6$ m.

Analytical Fokker-Planck models for collisional loss of fusion products near the passing/trapped boundary are also being developed to more accurately calculate the collisional loss at the specific poloidal angles for the lost ion detectors in TFTR. Preliminary results from one of these²³ models are that the ratio of the calculated collisional loss to the first-orbit loss at the 90° detector location is $\approx 1–3$ for 1 MeV tritons and $\approx 0.3–0.9$ for 3 MeV protons for a typical $R=2.45$ m, $I=1.6$ MA supershot. A collisional loss at the upper end of this range would result imply a loss signal about equal to the first-orbit loss signal, since these detectors are primarily sensitive to 3 MeV protons due to their larger energy.⁶ Thus the present calculations of collisional loss cannot quite account for the observed delayed loss, which is $\approx 2–4$ larger than the first-orbit loss at the 90° detector. Note that any collisional loss model would also need to account for the apparent *absence* of delayed loss in the 90° detector for $R=2.6$ m plasmas and at other poloidal angles for $R=2.45$ m plasmas.¹⁸

VII. ICRH-INDUCED LOSS

Several different interactions can occur between MeV ions and ICRH in TFTR. During H-minority heating in the power range $\approx 1–3.5$ MW without NBI there has been a loss of $\approx 0.5–1.0$ MeV hydrogen minority tail ions, particularly to the detectors $<45^\circ$ below the outer midplane.²⁴ This increases rapidly with ICRH power, and can be strongly modulated by sawteeth and other low-frequency MHD activity, such as $m=2$ modes. At higher ICRH powers there is an additional minority tail ion loss correlated with the appearance of high-frequency Alfvén waves, apparently due to a collective fast ion instability.²⁵ Since these effects occur with ICRH alone (without NBI), the lost ions are clearly due to the escape of a small fraction of the H-minority tail (since the fusion reaction rate is negligible).

Another ICRH scenario of interest is ³He minority heating experiments with NBI. This situation is more complicated, since there are several types of MeV ions in the plasma simultaneously, namely ³He tail ions (with a “temperature” of $\approx 0.5–1$ MeV), D–D fusion products, and D–³He fusion products (3.7 MeV alphas and 15 MeV protons). Nevertheless, a clear and reproducible increase of the MeV ion loss rate was observed during such ICRH experiments in both the 1990²⁶ and 1992²⁷ TFTR runs. This increase was interpreted as a sum of the first-orbit loss of D–³He fusion product alpha particles, plus an anomalous loss that was peaked strongly toward the 45° detector (the 20° detector could not be used in these experiments due to potential probe overheating). It was difficult to determine whether the anomalous part of the loss was either direct tail ion loss (as in H-minority heating) or ICRH-induced fusion product loss (either D–D tritons or protons or D–T alphas), since these loss detectors cannot distinguish particle species, but only their gyroradii.

An ICRH electron heating experiment was done in the 1992 run, which helped to clarify this situation by intentionally avoiding the creation of a minority tail population.²⁸ In this experiment a series of ≈ 2 MW pulses of ICRH were applied to a discharge with ≈ 23 MW of NBI. In these discharges, D–D fusion products were the only MeV ions present, and the ICRH could resonate with both 3 MeV protons and/or 1 MeV tritons. It was observed that at each ICRH pulse the loss of MeV ions increased by $\approx 25\%$ at the 90° detector, with smaller increases in the 60° and 45° detectors. These increases could only be due to an ICRH-induced loss of previously confined D–D fusion products, particularly since the increase occurred within ≈ 10 ms (far too short for MeV ion tail formation). The gyroradius distribution of this anomalous ICRH-induced D–D fusion product loss was similar to that of first-orbit loss, i.e., the ICRH appeared to expel fusion products near their birth energy. The pitch angle distribution of this anomalous loss in the 90° detector peaked near the passing-trapped boundary, consistent with marginally passing ions being given an additional perpendicular gyrovelocity by the ICRH, such that they entered the first-orbit loss cone.

Modeling of this ICRH-induced loss process has been done based on the expected ICRH-induced pitch angle scattering of fusion products.²³ Preliminary results suggest, at least, qualitative agreement with the measured loss during the electron heating experiment. Details of this calculation will be presented elsewhere.

VIII. SUMMARY AND CONCLUSION

Three mechanisms for the anomalous loss of D–D fusion products in TFTR have been described: MHD-induced, delayed loss, and ICRH-induced loss. The most serious of these seems to be due to coherent, low- n MHD activity, which has been seen to increase the loss by up to a factor of ≈ 5 –10 above the first-orbit loss level. Since the global first-orbit loss is calculated to be $\approx 3\%$ for discharges of this type, the estimated MHD-induced loss level can be up to $\approx 20\%$ – 30% . The delayed loss observed at the 90° detector is ≈ 2 –4 times the first-orbit loss level, but is quite reproducible, in contrast to the MHD-induced loss, which can vary dramatically from shot to shot. The ICRH-induced fusion product loss appears to be $\approx 25\%$ of the first-orbit loss level in those cases where this effect can be clearly isolated.

The main implication of these results for the TFTR D–T experiments is that large, low- n MHD activity should be avoided during experiments that require a large confined alpha particle population, such as alpha heating or collective alpha instability experiments. If such MHD activity can be avoided, the global loss fraction of alphas due to single-particle effects should be $< 20\%$.

The main implication of these results for future D–T experiments such as ITER is that the expected losses due to the “anomalous” single-particle effects of MHD activity and ICRH waves should be understood and calculated to ensure that the alpha loss fraction remains small. These calculations can be done in a preliminary form using the models being developed to understand the TFTR fusion

product losses, and can be checked using existing measurements of anomalous fusion product losses seen in other experiments.²⁹ In this way these “anomalous” effects can eventually become as well understood as the “classical” losses due to TF ripple, which have been fairly accurately verified by experiment.^{3,4,30,31}

ACKNOWLEDGMENTS

We thank the TFTR team for support for these experiments, and H. P. Furth, R. Hawryluk, K. McGuire, D. Meade, D. Mikkelsen, and K. M. Young, and D. J. Sigmar for discussions on alpha physics.

This work was performed under U.S. Department of Energy Contract No. DE-AC02-CHO-3073.

¹M. C. Zarnstorff, G. Bateman, S. H. Batha, M. Beer, M. G. Bell, R. E. Bell, H. Biglari, M. Bitter, R. Boivin, N. L. Bretz, R. V. Budny, C. E. Bush, J. D. Callen, Z. Chang, L. Chen, C. Z. Cheng, S. C. Cowley, D. S. Darrow, R. D. Durst, P. C. Efthimion, R. J. Fonck, E. D. Fredrickson, G. Y. Fu, H. P. Furth, G. J. Greene, B. Grek, L. R. Grisham, G. W. Hammett, R. J. Hawryluk, W. W. Heidbrink, K. W. Hill, S. P. Hirshman, D. J. Hoffman, J. C. Hosea, M. Hughes, R. A. Hulse, A. C. Janos, D. L. Jassby, F. C. Jobs, D. W. Johnson, L. C. Johnson, J. Kamperschroer, J. Kesner, H. Kugel, P. H. LaMarche, B. LeBlanc, F. Levinton, J. S. Machuzak, R. Majeski, D. M. Manos, D. K. Mansfield, E. S. Marmor, M. E. Mauel, E. Mazzucato, M. P. McCarthy, D. C. McCune, K. M. McGuire, D. M. Meade, S. S. Medley, D. R. Mikkelsen, D. A. Monticello, D. Mueller, M. Murakami, J. Murphy, Y. Nagayama, G. A. Navratil, R. Nazikian, D. K. Owens, H. K. Park, W. Park, S. F. Paul, F. W. Perkins, E. Perry, C. K. Phillips, M. Phillips, S. Pitcher, N. Pomphrey, D. A. Rasmussen, M. H. Redi, G. Rewoldt, F. Rimini, D. Roberts, A. L. Roquemore, S. A. Sabbagh, G. Schilling, J. Schivell, G. L. Schmidt, S. D. Scott, J. A. Snipes, J. E. Stevens, W. Stodiek, J. D. Strachan, B. C. Stratton, E. J. Synakowski, W. M. Tang, G. Taylor, J. L. Terry, M. Thompson, H. H. Towner, H. Tsui, M. Tuszewski, M. Ulrickson, S. Von Goeler, A. Von Halle, R. M. Wieland, M. Williams, J. R. Wilson, K. L. Wong, P. Woskov, G. A. Wurden, M. Yamada, K. M. Young, and S. J. Zweben, *Proceedings of the 14th International Conference on Plasma Physics and Controlled Nuclear Fusion Research*, Wurzburg (International Atomic Energy Agency Vienna, 1993), Paper A-2-2.

²S. J. Zweben, R. L. Boivin, C.-S. Chang, G. W. Hammett, and H. E. Mynick, *Nucl. Fusion* **31**, 2219 (1991).

³R. Boivin, S. J. Zweben, and R. B. White, *Nucl. Fusion* **33**, 449 (1993).

⁴R. Boivin and S. J. Zweben, *Phys. Fluids B* **5**, 1559 (1993).

⁵S. J. Zweben, R. Boivin, D. S. Darrow, E. D. Fredrickson, H. E. Mynick, R. B. White, H. Biglari, N. L. Bretz, R. V. Budny, C. E. Bush, C. S. Chang, L. Chen, C. Z. Cheng, R. Fisher, R. J. Fonck, G. Y. Fu, G. W. Hammett, R. J. Hawryluk, J. C. Hosea, L. C. Johnson, J. S. Machuzak, D. K. Mansfield, J. McChesney, K. M. McGuire, G. McKee, S. S. Medley, M. Murakami, R. Nazikian, D. K. Owens, H. K. Park, J. Park, C. K. Phillips, J. Schivell, B. C. Stratton, M. Tuszewski, M. Ulrickson, R. Wilson, P. Woskov, and K. M. Young, in Ref. 1, Paper A-6-3.

⁶R. Boivin, Z. Lin, A. L. Roquemore, and S. J. Zweben, *Rev. Sci. Instrum.* **63**, 1992 (4418).

⁷M. Tuszewski and S. Zweben, *Rev. Sci. Instrum.* **64**, 2459 (1993).

⁸S. J. Zweben, R. L. Boivin, R. E. Duvall, E. D. Fredrickson, R. J. Goldston, H. E. Mynick, J. D. Strachan, and R. B. White, *Phys. Fluids B* **2**, 1411 (1990).

⁹See National Technical Information Service Document No. DE93040431 [S. J. Zweben, D. S. Darrow, R. V. Budny, Z. Chang, C. Z. Cheng, E. D. Fredrickson, H. W. Herrmann, H. E. Mynick, and J. Schivell, “Recent progress on MHD-induced loss of D–D fusion products in TFTR,” Princeton Plasma Physics Laboratory (PPPL) Report No. 2934, Aug. 1993]. Copies may be ordered from NTIS, Springfield, VA 22161.

¹⁰See National Technical Information Service Document No. DE94001717 [Z. Chang, E. D. Fredrickson, J. D. Callen, K. M. McGuire, M. G. Bell, R. V. Budny, C. E. Bush, D. S. Darrow, A. C.

- Janos, L. C. Johnson, H. Park, S. D. Scott, J. D. Strachan, E. J. Synakowski, G. Taylor, R. M. Wieland, M. C. Zarnstorff, S. J. Zweben, and the TFTR group, "Transport effects of los (m,n) modes on TFTR supershots," PPPL-2941, 1993]. Copies may be ordered from NTIS, Springfield, VA 22161.
- ¹¹E. D. Fredrickson, K. McGuire, A. Cavallo, B. Grek, D. W. Johnson, and A. W. Morris, *Rev. Sci. Instrum.* **59**, 1797 (1988).
 - ¹²D. S. Darrow, E. D. Fredrickson, H. E. Mynick, R. Nazikian, R. B. White, K.-L. Wong, and S. J. Zweben, *Proceedings of the 19th EPS Conference on Controlled Fusion and Plasma Physics*, Amsterdam, 1992 (European Physical Society, Amsterdam, 1992), p. 1-431.
 - ¹³D. S. Darrow, S. J. Zweben, Z. Chang, C. Z. Cheng, E. D. Fredrickson, E. Mazzucato, R. Nazikian, C.-K. Phillips, R. B. White, J. R. Wilson, and K.-L. Wong, *Proceedings of the IAEA Technical Committee Meeting on Alpha Particles in Fusion Research*, Trieste, Italy 1993 (International Atomic Energy Agency, Vienna, 1993), p. 27.
 - ¹⁴C. Z. Cheng, G. Y. Fu, H. E. Mynick, R. V. Budny, R. B. White, S. J. Zweben, C. T. Hsu, D. J. Sigmar, D. A. Spong, B. A. Carreras, and C. L. Hedrick, in Ref. 1, Paper D-2-1.
 - ¹⁵L. Johnson, (private communication, 1993).
 - ¹⁶H. E. Mynick, *Phys. Fluids B* **5**, 1471 (1993).
 - ¹⁷R. B. White and H. E. Mynick, *Phys. Fluids B* **1**, 980 (1989).
 - ¹⁸S. J. Zweben, D. S. Darrow, E. D. Fredrickson, and H. E. Mynick, *Nucl. Fusion* **33**, 705 (1993).
 - ¹⁹C. T. Hsu, P. J. Catto, and D. J. Sigmar, *Phys. Fluids B* **2**, 280 (1990).
 - ²⁰V. Ya. Goloborod'ko and V. O. Yavorski, *Proceedings of the IAEA Technical Committee Meeting on Alpha Particles in Fusion Research*, Trieste, Italy 1993 (International Atomic Energy Agency, Vienna, 1993), p. 490.
 - ²¹R. V. Budny, "A standard DT supershot simulation," to appear in *Nucl. Fusion*
 - ²²M. H. Redi, *Bull. Am Phys. Soc.* **38**, 2037 (1993).
 - ²³C. S. Chang (private communication, 1993).
 - ²⁴See National Technical Information Service Document No. DE91010043 (J. C. Hosea, C. K. Phillips, J. E. Stevens, J. R. Wilson, M. Bell, R. Boivin, A. Cavallo, P. Colestock, E. Fredrickson, G. Hammett, D. Hoffman, H. Hsuan, A. Janos, D. Jassby, F. Jobs, K. McGuire, D. Mueller, Y. Nagayama, K. Owens, H. Park, G. Schmidt, B. Stratton, G. Taylor, K. L. Wong, S. Zweben, and the TFTR Group, "ICRF Satwooth Stabilization—Application on TFTR and CIT," PPPL-2738, 1991). Copies may be ordered from NTIS, Springfield, VA 22161.
 - ²⁵J. R. Wilson, M. G. Bell, H. Biglari, M. Bitter, N. L. Bretz, R. V. Budny, C. E. Bush, Z. Chang, L. Chen, D. S. Darrow, P. C. Efthimion, E. D. Fredrickson, G. Y. Fu, R. C. Goldfinger, B. Grek, L. R. Grisham, G. W. Hammett, R. J. Hawryluk, D. J. Hoffman, J. C. Hosea, A. C. Janos, D. L. Jassby, F. C. Jobs, D. W. Johnson, L. C. Johnson, J. S. Machuzak, R. Majeski, D. K. Mansfield, E. Mazzucato, K. M. McGuire, S. S. Medley, D. Mueller, M. Murakami, R. Nazikian, D. K. Owens, H. K. Park, S. F. Paul, C. K. Phillips, A. T. Ramsey, D. A. Rasmussen, F. Rimini, J. H. Rogers, A. L. Roquemore, G. Schilling, J. Schivell, G. L. Schmidt, J. E. Stevens, J. D. Strachan, B. C. Stratton, E. J. Synakowski, G. Taylor, M. Ulrickson, K. L. Wong, M. Yamada, K. M. Young, M. C. Zarnstorff, and S. J. Zweben, in Ref. 1, Paper E-2-2.
 - ²⁶S. J. Zweben, G. W. Hammett, R. L. Boivin, C.-K. Phillips, and J. R. Wilson, *Nucl. Fusion* **32**, 1823 (1992).
 - ²⁷G. Taylor, M. G. Bell, H. Biglari, M. Bitter, N. L. Bretz, R. Budny, L. Chen, D. Darrow, P. C. Efthimion, D. Ernst, E. Fredrickson, G. Y. Fu, B. Grek, L. Grisham, G. Hammett, J. C. Hosea, A. Janos, D. Jassby, F. C. Jobs, D. W. Johnson, L. C. Johnson, R. Majeski, D. K. Mansfield, E. Mazzucato, S. S. Medley, D. Mueller, R. Nazikian, D. K. Owens, S. Paul, H. Park, C. K. Phillips, J. H. Rogers, G. Schilling, J. Schivell, G. L. Schmidt, J. E. Stevens, B. C. Stratton, J. D. Strachan, E. Synakowski, J. R. Wilson, K. L. Wong, S. J. Zweben, L. Baylor, C. E. Bush, R. C. Goldfinger, D. J. Hoffman, M. Murakami, A. L. Qualls, D. Rasmussen, J. Machuzak, F. Rimini, and Z. Chang, "Ion cyclotron range of frequency heating on the tokamak fusion test reactor," to appear in *Plasma Phys. Controlled Nucl. Fusion Res.*
 - ²⁸M. Murakami, E. Fredrickson, E. F. Jaeger, D. A. Rasmussen, F. G. Rimini, J. R. Wilson, M. C. Zarnstorff, D. B. Batchelor, M. G. Bell, R. Budny, C. E. Bush, D. Darrow, R. C. Goldfinger, D. J. Hoffman, J. C. Hosea, A. Janos, R. Majeski, D. Mansfield, H. Park, C. K. Phillips, J. H. Rogers, S. Sabbagh, G. Schilling, S. C. Scott, J. E. Stevens, E. Synakowski, G. Taylor, R. W. Wieland, and S. Zweben, *Proceedings of the 20th EPS Conference on Controlled Fusion and Plasma Physics*, European Physical Society, Lisbon (European Physical Society, Petit-Lancy, 1993), Paper 5-34.
 - ²⁹H. H. Duong and W. W. Heidbrink, *Nucl. Fusion* **33**, 211 (1993).
 - ³⁰K. Tobita, K. Tani, Y. Neyatani, A. A. E. van Blokland, S. Miura, T. Fujita, H. Takahashi, T. Nishitani, M. Matsuoka, and S. Takechi, *Phys. Rev. Lett.* **69**, 3060 (1992).
 - ³¹B. Tubbing and the JET Team, in Ref. 28, Paper 1-10.

COMMENTS

Comments refer to papers published in Physics of Plasmas and are subject to a length limitation of two printed pages. The Board of Editors will not hold itself responsible for the opinions expressed in the Comments.

Erratum: "A short mean free path, coupled neutral-ion transport description of a tokamak edge plasma" [Phys. Plasmas 1, 1936 (1994)]

Peter J. Catto

Massachusetts Institute of Technology, Plasma Fusion Center, 167 Albany Street, NW16-236, Cambridge, Massachusetts 02139

(Received 10 June 1994; accepted 10 June 1994)

A sign error occurs on the right side of the neutral and ion energy conservation equations in the terms proportional to the charge exchange frequency ν_x . The sign between the $3(T-\tau)/2$ and $M(V^2-U^2)/2$ terms should be positive so that the quantity in the large parentheses on the right side of Eqs. (61) and (70) should be

$$\left(\frac{3}{2} (T-\tau) + \frac{1}{2} M(V^2-U^2) \right).$$

Erratum: "Anomalous losses of deuterium–deuterium fusion products in the Tokamak Fusion Test Reactor" [Phys. Plasmas 1, 1469 (1994)]

S. J. Zweben, D. S. Darrow, H. Herrmann, M. Bell, R. Boivin, R. V. Budny, C. E. Bush, C. S. Chang, C. Z. Cheng, D. Ernst, E. D. Fredrickson, G. Hammelt, L. C. Johnson, D. McCune, M. Murakami, H. E. Mynick, D. K. Owens, J. Park, C. K. Phillips, M. H. Redi, J. Schivell, S. Scott, J. Strachan, G. Taylor, M. Tuszewski, R. B. White, J. R. Wilson, and M. Zarnstorff

Princeton Plasma Physics Laboratory, P.O. Box 451, Princeton, New Jersey 08543

(Received 13 June 1994; accepted 13 June 1994)

The third column of Table I should be headed " $\tau_{\text{scat}}/\tau_{\text{slow}}$ " instead of " $\tau_{\text{slow}}/\tau_{\text{scat}}$ " and in the paragraph on p. 1476 beginning "The relevant time scales...", the phrase "10 times larger" should be replaced by "10 times smaller."